In-situ infrared spectroscopic studies of hydroxyl in amphiboles at high pressure

Elizabeth C. Thompson[1,*], Andrew J. Campbell[1], Zhenxian Liu[2]

[1]Department of the Geophysical Sciences, University of Chicago, 5734 S. Ellis Avenue, Chicago, Illinois 60637, U.S.A., [2]Geophysical Laboratory, Carnegie Institution of Washington, 5251 Broad Branch Road NW, Washington, D.C. 20015, U.S.A.

*Corresponding author. Tel: +1 504 460 7658

Email: ecthompson@uchicago.edu (E. C. Thompson)

Submitted to *Am. Mineral.* June 15, 2015

Accepted by *Am. Mineral*. October 27, 2015

Abstract

Oceanic plates contain numerous hydrous phases including amphiboles, which are important carriers of water into subduction zones. The hydroxyl bound within the crystalline structure of hydrous minerals, as well as changes in hydrogen bond symmetry, can impact the bulk properties of these minerals. In this study, twelve natural amphibole samples spanning a range of ten compositions were probed with synchrotron infrared spectroscopy at room temperature and pressures up to 60 GPa. Infrared spectra were collected at atmospheric pressure and at regular intervals during compression, allowing for the collection of spectra centered on the typical O-H stretching region at 3600-3700 cm^{-1} as they evolved with pressure for each composition. The number of O-H bands within each sample was found to vary with composition, but the pressure dependence of O-H frequency shifting more closely correlated with mode frequency at ambient pressure than with composition. Combined with earlier results, these data reveal a linear relationship between mode frequency at ambient pressure and pressure dependence of O-H stretching modes in amphiboles and sheet silicates.

Two sample preparation methods utilized in this study allowed for direct comparison between quasi-hydrostatic neon-loaded sample conditions and the conditions achieved with a KBr pressure medium. Samples loaded in neon preserved sharper peaks, allowing greater spectral resolution, especially at higher pressures when peaks are most likely to broaden or disappear due to crystalline disorder and pressure gradients across the sample. This new quasi-hydrostatic loading method proved valuable to tracing O-H stretching behavior in amphiboles to higher pressures than previously obtained and will lend itself to future study of O-H stretching pressure dependence in a wide range of hydrous minerals.

Keywords: infrared, high pressure, diamond anvil cell, hydroxyl, amphiboles

Introduction

Oceanic plates contain numerous hydrous phases, and since amphiboles contain ~2 wt.% H_2O they are important carriers of water into subduction zones (Stern 2002). As amphiboles within the oceanic slab are subjected to increasing temperatures and pressures as the slab subducts along the cold slab geotherm, a dehydration reaction is initiated. The dehydration of amphiboles may extend to depths of 100 km, depending on local variations in the subducting slab's geotherm (Stern 2002). This reaction influences island arc volcanism, as 5-20% of the water released from subducting basaltic slabs into overlaying mantle may originate from amphibole dehydration (Schmidt and Poli 1998). The accommodation and subsequent loss of this hydroxyl at elevated pressure has been predicted to vary with composition in response to the repulsive interactions between cations, as well as the influence on hydrogen bonding by next-to-nearest neighbors, in a chemically complex system which merits further study (Hawthorne and Della Ventura 2007). Hydrogen cycling in the Earth's interior is critical due to the influence of hydroxyl on melting temperatures, rheology, electrical conductivity, and atomic diffusivity, as well as macro-scale phenomena including plate tectonics and volcanism (Hofmeister 2004; Hirschmann 2006). Lastly, hydrogen bond symmetrization in hydrous minerals may influence the response of bulk properties to pressure, for example increasing bulk modulus by as much as ~20% (Tsuchiya et al. 2005; Sano-Furukawa et al. 2009; Husher et al. 2011).

Amphiboles are a group of inosilicates that accommodate an extensive range of both cation and anion substitutions ($AB_2C_5T_8O_{22}W_2$), resulting in classification into eight sub-groups (Hawthorne et al. 2012). In this generalized formula the large A site may contain a cation (e.g., Na, Ca, etc.) but is often vacant, the B represents the cations of the M4 site which may be 6 or 8-

fold coordinated, and the C represents the cations of the octahedral M1, M2, and M3 sites. Structurally, amphiboles are comprised of corner-linked double chains of silicate tetrahedra (T sites) that extend along the *c*-axis and bookend a single octahedral strip. Oxygens occupy two distinct planes; basal or bridging oxygen link adjacent $(SiO_4)^{4-}$ tetrahedra along the *c*-axis and apical or non-bridging oxygen are coordinated to single tetrahedra. The A site between the octahedral and tetrahedral strips (also A in the generalized formula above) can host large alkali ions such as Na^+ and K^+ but often remains vacant. Three sites within the inner octahedral strip accommodate divalent and trivalent cations including Al, Ca, Fe, Mg, and Ti, and are represented by B and C in the generalized formula. The W site hosts OH^- or halogens. The amphibole family is divided into two symmetries; monoclinic and orthorhombic, and five structures; *C2/m*, *P2$_1$/m*, *P2/a*, *Pnma*, *Pnmn*, of which the first four occur in natural samples. The natural specimens used in this study represent the four most common rock-forming compositional subgroups and both symmetry groups.

Infrared (IR) spectroscopy allows direct detection of the O-H covalent bond stretching frequency within a hydrogen bond (O-H…O). Considering the stretching vibration as a simple harmonic oscillator it has been shown that the frequency of an idealized relaxed hydroxyl bond is 3600 cm^{-1} at ambient pressure, with deviations from this frequency as the result of changing the strength of the bond (Huggins and Pimental 1956). It has been observed that O-H stretching bands above a 1-bar frequency of ~3600 cm^{-1} are likely to increase in bond frequency with pressure while those below this set point are likely to decrease with pressure (Cynn and Hofmeister 1994). Yet, the hydroxyls within amphiboles are not isolated, therefore instead of a simple two mass harmonic problem, there is a potential for influence by nearest and next nearest neighbors. Additionally, the local environment of the hydroxyl site, including geometry, cation

occupation, defect structure, and compression behavior influence O-H stretching pressure dependencies, potentially causing significant deviations from this trend (e.g., Koch-Müller et al. 2003; Jahn et al. 2012). The wide range of amphibole compositions in this study was chosen to investigate whether composition has a primary influence on the pressure dependence of individual O-H stretching modes in amphiboles.

Experimental Methods

Twelve natural amphibole samples spanning ten distinct compositions were characterized using energy dispersive X-ray spectroscopy (EDS) as shown in Table 1. Subsequently, pieces of each amphibole composition were ground in an agate mortar and pestle, mixed in a 1:1 molar ratio with KBr, homogenized in a ball mill for 45 minutes at 20 Hz, and pressed into ~5-10 μm thick platelets to load into symmetric-type diamond anvil cells (DACs). All sample powders were either kept in a desiccator prior to loading or were baked for 30-60 minutes at 375 K before being compressed into pellets. Small ruby grains placed in the sample chamber enabled in situ pressure monitoring using the R_1 luminescence line (Mao et al. 1978). Gaskets of stainless steel or rhenium were used, with sample chambers of 80 μm or 50 μm diameter, respectively.

The two sample geometries used in this study are shown in Figure 1b and 1c. The first sample set-up utilized 10 μm thick platelets of KBr as non-hydrostatic pressure medium, surrounding the sample platelet of mixed amphibole + KBr following a methodology previously described by Robert et al. (1989). Mixing the sample material with dehydrated KBr mitigated the preferential orientation of amphibole grains during compression and limited the likelihood of saturated absorption peaks in the IR spectra. The second sample assembly also employed mixed amphibole + KBr platelets, but replaced the KBr pressure medium with a nearly hydrostatic neon

pressure medium, which was loaded as a pressurized gas at the Advanced Photon Source using the COMPRES/GSECARS gas-loading system (Rivers et al. 2008). After loading the mixed KBr + amphibole platelets, but prior to closing the DACs, prepared sample assemblies were baked for an additional hour at 375 K to mitigate the effect of water vapor absorption (Jenkins et al. 2013), which can overwhelm the signal of structural hydroxyl.

Diamond anvils cells with 250 μm culet sizes were used to pressurize the samples. All high-pressure synchrotron infrared spectra in this study were collected at the U2A beamline of the National Synchrotron Light Source at the Brookhaven National Laboratory using either a Bruker Vertex 80v FTIR spectrometer with Hyperion 2000 microscope, or a Bruker IFS/66v FTIR spectrometer with custom microscope, both with HgCdTe detectors. Different spectral resolutions of 1 cm^{-1}, 2 cm^{-1}, and 4 cm^{-1} were tested for the lowest pressure spectra and no significant differences in the quality of data was found, therefore 4 cm^{-1} resolution was applied to all spectra. The spectra presented here were recorded in 1024 or 512 scans. PeakFit (Systat Software) was used for background subtraction and to obtain precise absorption peak positions using a least-squares refinement within the hydroxyl absorption region of interest following a previously published methodology (Hawthorne et al. 1997).

Results and Discussion

Room temperature infrared spectra were collected at atmospheric pressure and at regular intervals during compression until individual absorption bands were obscured by peak broadening consistent with non-hydrostatic stresses (Lager et al. 2005). Samples that contained peaks that were broad at atmospheric pressure, because of increased local cation substitution (Strens 1974; Noguchi et al. 2012), were monitored until all peaks became impossible to track.

For most samples additional spectra were collected at regular intervals during DAC decompression. In all such cases the position of absorption bands returned to original atmospheric pressure conditions, although there were varying degrees of hysteresis in the decompression frequencies compared to the frequency at similar pressures on initial compression, as has been seen in a previous Raman study (Shim et al. 2006). The elapsed time between decompressing the sample and acquiring the spectra did not influence the degree of hysteresis. When determining the pressure dependence of individual stretching modes, only the frequencies measured during compression were used. The IR absorption peak positions are listed in Supplementary Table 1.

Although individual absorption peaks broadened at high pressures, no samples exhibited the gradual pressure-induced band-splitting that has been previously used to interpret symmetry changes (Yang et al. 1998). Depending on the composition and symmetry of each amphibole, samples exhibited between one and four distinct hydroxyl bands (Figure 2), identified here as bands A, B, C, and D following the terminology of Hawthorne and Della Ventura (2007). Individual stretching bands are due not to a change in the location of the hydrogen, but rather nonequivalent bond lengths. Coexisting bands may exist due to variations in local M1 and M3 occupancy, with additional fine structure due to variations in the M2 and A sites (Hawthorne and Della Ventura 2007). The number of observed bands may in fact be fewer than the actual number of absorption frequencies as closely overlapping absorption peaks may present as peak broadening (Hawthorne and Della Ventura 2007).

The frequency of each stretching band during compression is plotted against pressure for each of the twelve samples, spanning ten compositions, in Figure 3. Despite small offsets due to deviations in chemical composition (Oberti et al. 2007), it is quite possible to compare

frequencies between different amphibole samples at similar pressures for all four hydroxyl bands (Figure 2). Two main features are evident; firstly peak positions are very comparable between compositions at similar pressures across all bands (within 10 cm^{-1} at low pressure, with increasing spread at increased pressure), and secondly the pressure dependence of these bands is markedly consistent across a wide range of compositions (Figure 3). Considering that this data includes ten distinct compositions, nearest neighbor cations do not seem to have a primary influence on the pressure dependence of the O-H stretching modes in amphiboles. The change in pressure dependence of the anthophyllite (L31) A-band above 30 GPa may be due to a previously undetected symmetry change or developing deviatoric stresses within that sample. Similarly, a nonlinear trend appears in the pressure dependence of the arfvedsonite (L30) D-band at pressures exceeding 20 GPa.

Overall there was good agreement between samples loaded with both pressure media, but Ne-loaded samples exhibited sharper absorption peaks to higher pressure, indicating that the greater hydrostaticity from this sample loading method minimized stress-induced peak broadening (Figure 4). Although the pressures achieved in this study greatly exceed the range of amphibole stability expected under geologic conditions, this method does enable the pressure dependence to be more precisely defined, providing greater insight into the physical mechanisms and systematics of pressure dependence in amphibole O-H stretching modes. Pressure dependences (Table 2) were determined by a linear fit to the pressure-frequency data of each O-H stretching band of each composition in the study up to 20 GPa.

These pressure dependences are plotted in Figure 5 against the initial 1-bar frequency of each band. Interestingly, there is a near-linear correlation between the 1-bar O-H stretching frequency and its pressure dependence in these amphiboles. The results of high-pressure IR

absorption studies on other amphiboles (Yang et al. 1998; Iezzi et al. 2008) likewise follow the linear relationship found among the amphibole O-H stretching modes reported here. It has been observed previously that in certain minerals, higher 1-bar O-H stretching frequencies have positive pressure dependence and lower 1-bar O-H stretching frequencies have negative pressure dependence (Prewitt and Parise 2000; Yang et al. 2014). Similar to the findings of this study, Cynn and Hofmeister (1994) showed that the various O-H stretching modes within hydrous wadsleyite have pressure-dependences that are linearly related to their 1-bar frequencies. Based on our new data, we conclude that a similar correlation exists between 1-bar O-H frequencies and their pressure dependences are within the amphibole group. The 1-bar frequency from this study corresponding to the cut-off between positive and negative pressure dependence is ~3640 cm^{-1}. This pressure-independent frequency is coincident with previous experimental results (Cynn and Hofmeister 1994) and the free oscillation parameter from the simple harmonic oscillator model.

The ability to correlate 1-bar hydroxyl vibration frequency with pressure dependence enables the prediction of either bond strengthening or softening. Bands with initial frequencies above the zero pressure-dependence threshold will shorten with increasing pressure, associated with greater force constant of the O-H bond. In amphiboles only bands that lie below the 3640 cm^{-1} threshold would plausibly symmetrize with pressure. In other words, only in the case of a band with negative frequency shift pressure-dependence can the double well potential of the H atom evolve with increased pressure to a single well potential minimum resulting in the H atom half way between the donor and acceptor oxygens (Prewitt and Parise 2000). In short, mode frequency at ambient pressure, rather than composition is the primary factor controlling the pressure dependence of individual stretching modes. Still, composition likely plays an important

role, as 1-bar frequencies (i.e. presence of the A, B, C, and/or D bands) are a function of nearest neighbor and next-to-nearest neighbor occupancies.

Hydroxyl ions (OH^-) within amphiboles are generally accommodated along the octahedral strip at the non-tetrahedral oxygen site, which is very similar to the OH^- site in *t–o–t* phyllosilicates (e.g. talc, micas). As shown in Figure 5, the O-H bonds within these comparable sites in amphiboles and *t–o–t* phyllosilicates largely exhibit the same linear relationship between pressure dependence and 1-bar frequency. This consistency in the high-pressure dependence of their O-H stretching frequencies is due to the similarity in the local environments of the hydroxyl in these minerals. Still, even within ino- and phyllosilicates, O-H stretching modes are not always so simply accommodated, as can be seen in the low frequency biotite datum from Williams et al. (2012), which the author attributed to an additional hydroxyl stretching mode juxtaposed with an octahedral vacancy. This may or may not be the case, as in Figure 5 the datum for muscovite, whose octahedral strip contains systematic vacancies, clusters with the data for trioctahedral minerals (having fully-occupied octahedral sites).

Many other minerals incorporate hydroxyl on sites that are not equivalent to that in amphiboles (and *t–o–t* phyllosilicates), and in these minerals one should not expect that the pressure dependences of the O-H stretching modes would exhibit the same relationship to mode frequency at ambient pressure. Indeed, as shown in Figure 6, minerals such as wadsleyite, ringwoodite, superhydrous phase B (shy-B), and hydrous post-perovskite (hy-ppv) do not lie along the amphibole trends but exhibit different pressure dependence behavior because of the differences in the local environment of hydroxyl within their structures. Some minerals accommodate hydroxyl both in an amphibole-like site (i.e. at the non-tetrahedral oxygens within the *t–o* structure) and in one or more additional non-equivalent sites. In the example of the

serpentine group (Figure 6), the observed pressure dependences of some O-H stretching modes cluster well within those of the amphiboles, and others lie slightly outside the range described by the amphiboles.

In Figure 6, the observed correlation between 1-bar O-H stretching frequencies and their pressure dependences in amphiboles is shown in the larger context of minerals that host hydrogen in a variety of crystallographic environments. Obviously the correlation among amphiboles (and in phyllosilicates) does not extend to all OH-bearing minerals. The correlation described here (and in Figure 5) was identifiable in amphiboles and *t–o–t* phyllosilicates because of the wide compositional range over which high pressure IR absorption data were obtained for these mineral groups. It is reasonable to anticipate that O-H stretching modes in other mineral structures might also exhibit systematics among their pressure dependences that have so far remained unrealized because of the limited data available.

Using the high-resolution IR spectra available from this study, the relationship between frequency and pressure as a proxy for bond length within amphiboles was also investigated. Tremolite was singled out for this analysis, because as a near end-member composition it is particularly well-characterized even at high pressures. In this study three tremolite samples (L13, L14, L32), of two naturally occurring compositions, were compressed to pressures of 56, 37, and 45.4 GPa respectively. O-H bond lengths were calculated using an isothermal bulk modulus (K_T) of 85 GPa from Comodi et al. (1991), a pressure derivative of the bulk modulus (K_T') fixed to 4, an estimated unit-cell volume of 90 Å^3, and a 1-bar O-H bond length of 0.957 Å (Hawthorne and Grundy, 1976) using a Vinet equation of state (Vinet et al. 1987) of the form:

$$P_{300}(V) = 3K_T\left(\frac{1-\eta}{\eta^2}\right)e^{\frac{3}{2}(K_T'-1)(1-\eta)}$$

in which $\eta = (V/V_0)^{1/3}$ and initial volume is V_0. The O-H bond length was assumed here to vary as the cube root of unit-cell volume, although it should be noted that tremolite does exhibit anisotropic compression (Comodi et al. 1991). Calculated pressures were matched to pressures obtained from the R_1 luminescence line of ruby placed within the sample chamber of the diamond anvil cell. Badger (1934) proposed a general relationship between internuclear distance (r_e) and force constant (k_0) in binary molecules, as:

$$k_0\left(r_e - d_{ij}\right)^3 = 1.86$$

in which k_0 is given in N/cm, r_e is in Angstroms, and d_{ij} is a constant characteristic of a diatomic molecule with one element in the *ith* row and one element in the *jth* row. Oscillator frequency (ω) scales as k_0^2, so this equation suggests a linear relationship between $\omega^{-2/3}$ and r_e. As shown in Figure 7, Badger's rule accurately describes the relationship between frequency and calculated bond length that we obtain from our tremolite data.

Implications

Pressure induced hydrogen bond symmetrization, i.e. the shift from an asymmetric bonding configuration (O–H···O) to one in which the hydrogen is equidistant between two oxygens (O–H–O), has previously been detected in OH-bearing minerals (e.g., Xu et al. 2013). Our findings support and enhance previous observations that O-H bonds with high frequency stretching modes strengthen with pressure and are unlikely to participate in hydrogen bond symmetrization, whereas O-H bonds with low frequency stretching modes may soften with pressure. Furthermore, our findings demonstrate a relationship, linear over the range of minerals studied, between pressure shift and 1-bar frequency of the O-H modes in amphiboles. Neither composition nor symmetry plays a primary role in the pressure dependence of O-H stretching

modes within this study. Additionally, a comparison of our findings to *t–o–t* phyllosilicate minerals (Figure 5), suggest that the stretching frequency at 1 bar is strongly associated with pressure dependence in O-H stretching in phyllosilicates as well. We propose that other structural groups of minerals might also show a clear relationship between 1 bar O-H stretching frequency and its pressure derivative, distinct from that shown for amphiboles. These relationships might be revealed through further systematic studies. Future high-pressure IR spectroscopy of hydrous minerals with improved spectral resolution, and especially single-crystal studies, would allow for a more refined understanding of the details of this relationship as a function of local hydroxyl environment.

Our findings were in part enabled by our novel sample preparation technique, which improved the IR spectral resolution at higher pressures and enabled the simultaneous collection of well-defined Si-O and O-H stretching data at high pressure. Compared to the non-hydrostatic conditions achieved with a KBr pressure medium, the quasi-hydrostatic conditions of a neon-loaded sample preserved much more sharply defined peaks, which proved essential to capturing the pressure dependence of O-H band frequency at high pressures (Figure 4). Technical advancements to preserve high spectroscopic resolution are increasingly important as increased pressures introduce complicating but unavoidable factors including structural disorder and pressure gradients within the measured sample. This new method will lend itself to the study of O-H stretching in a wide range of hydrous and nominally anhydrous minerals.

Acknowledgments

We thank the editors and the two reviewers for their helpful comments on the manuscript. This material is based upon work supported by National Science Foundation Graduate Research

Fellowship under Grant # DGE-1144082 and National Science Foundation Grant # EAR-1427123. The U2A beamline at the National Synchrotron Light Source beamline is supported by COMPRES, the Consortium for Materials Properties Research in Earth Sciences under NSF Cooperative Agreement EAR 11-43050 and by the U.S. Department of Energy, Office of Science, Office of Basic Energy Sciences, under Contract # DE-AC02-98CH10886. Use of the COMPRES-GSECARS gas loading system was supported by COMPRES under NSF Cooperative Agreement EAR 11-57758 and by GSECARS through NSF grant EAR-1128799 and DOE grant DE-FG02-94ER14466. This research used resources of the Advanced Photon Source, a U.S. Department of Energy (DOE) Office of Science User Facility operated for the DOE Office of Science by Argonne National Laboratory under Contract No. DE-AC02-06CH11357.

References Cited

Ahrens, T.J. (1989) Water storage in the mantle. Nature, 342, 122–123.

Auzende, A.L., Daniel, I., Reynard, B., Lemaire, C., and Guyot, F. (2004) High-pressure behaviour of serpentine minerals: A Raman spectroscopic study. Physics and Chemistry of Minerals, 31, 269–277.

Badger, R.M. (1934) The Relation between Internuclear Distances and Bond Force Constants. Journal of Chemical Physics, 2, 128–131.

Comodi, P., Mellini, M., Ungaretti, L., and Zanazzi, P.F. (1991) Compressibility and high pressure structure refinement of tremolite, pargasite and glaucophane. European Journal of Mineralogy, 3, 485–499.

Cynn, H., Hofmeister, A. M. (1994) High-pressure IR spectra of lattice modes and OH vibrations in Fe-bearing wadsleyite. Journal of Geophysical Research, 99, 717–727.

Cynn, H., Hofmeister, A. M., Burnley, P.C., and Navrotsky, A. (1996) Thermodynamic properties and hydrogen speciation from vibrational spectra of dense hydrous magnesium silicates. Physics and Chemistry of Minerals, 23, 361–376.

Hawthorne, F.C. and Grundy, H.D. (1976) The crystal chemistry of amphiboles. IV. X-ray and neutron refinements of the crystal structure of tremolite. Canadian Mineralogist, 14, 334-335.

Hawthorne, F.C., Della Ventura, G., Robert, J.-L., Welch, M.D., Raudsepp, M., and Jenkins, D.M. (1997) A Rietveld and infrared study of synthetic amphiboles along the potassium-richterite-tremolite join. American Mineralogist, 82, 708–716.

Hawthorne, F.C., and Della Ventura, G. (2007) Short-Range Order in Amphiboles. Reviews in Mineralogy and Geochemistry, 67, 173–222.

Hawthorne, F. C., Oberti, R., Harlow, G. E., Maresch, W. V., Martin, R. F., Schumacher, J. C., Welch, M. D. (2012) IMA Report: Nomenclature of the amphibole supergroup. American Mineralogist, 97, 2031-2048.

Hirschmann, M.M. (2006) Water, Melting, and the Deep Earth H_2O Cycle. Annual Review of Earth and Planetary Sciences, 34, 629–653.

Hirschmann, M., and Kohlstedt, D. (2012) Water in Earth's mantle. Physics Today, 65, 40.

Hofmeister, A.M. (2004) Enhancement of radiative transfer in the upper mantle by OH- in minerals. Physics of the Earth and Planetary Interiors, 146, 483–495.

Huggins, C., and Pimentel, G. (1956) Systematics of the infrared spectral properties of hydrogen bonding systems: frequency shift, half width and intensity. The Journal of Physical Chemistry, 1129, 265–266.

Hushur, A., Manghnani, M.H., Smyth, J.R., Williams, Q., Hellebrand, E., Lonappan, D., Ye, Y., Dera, P., and Frost, D.J. (2011) Hydrogen bond symmetrization and equation of state of phase D. Journal of Geophysical Research, 116, B06203.

Iezzi, G., Liu, Z., and Della Ventura, G. (2006) Synchrotron infrared spectroscopy of synthetic $Na(NaMg)Mg_5SiO_8O_{22}(OH)_2$ up to 30 GPa: Insight on a new high-pressure amphibole polymorph. American Mineralogist, 91, 479–482.

Iezzi, G., Liu, Z., and Della Ventura, G. (2008) Synthetic $^{A}Na^{B}(Na_xLi_{1-x}Mg_1)^{C}Mg_5Si_8O_{22}(OH)_2$ (with x = 0.6, 0.2 and 0) $P2_1/m$ amphiboles at high pressure: a synchrotron infrared study. Physics and Chemistry of Minerals, 36, 343–354.

Jahn, S., Wunder, B., Koch-Müller, M., Tarrieu, L., Pohle, M., Watenphul, A., and Taran, M.N. (2012) Pressure-induced hydrogen bond symmetrization in guyanaite, beta-CrOOH: evidence from spectroscopy and ab initio simulations. European Journal of Mineralogy, 24, 839-850.

Jenkins, D.M., Della Ventura, G., Oberti, R., and Bozhilov, K. (2013) Synthesis and characterization of amphiboles along the tremolite-glaucophane join. American Mineralogist, 98, 588-600.

Koch-Müller, M., Dera, P., Fei, Y., Reno, B., Sobolev, N., Hauri, E., and Wysoczanski, R. (2003) OH^- in synthetic and natural coesite. American Mineralogist, 88, 1436-1445.

Lager, A.G., Marshall, W.G., Liu, Z. Downs, R.T. (2005) Re-examination of the hydrogarnet structure at high pressure using neutron powder diffraction and infrared spectroscopy. American Mineralogist, 90, 639–644.

Ma, M., Liu, W., Chen, Z., Liu, Z., and Li, B. (2012) Compression and structure of brucite to 31 GPa from synchrotron X-ray diffraction and infrared spectroscopy studies. American Mineralogist, 98, 33–40.

Mashino, I., Murakami, M., Ohtani, E. (2014) Sound velocity of δ-AlOOH up to core-mantle boundary pressures: Implications for the seismic anomalies induced by hydrated sediment in subducting slabs, AGU Fall Meeting, San Francisco, CA.

Mao, H.K., Bell, P.M., Shaner, J.W., and Steinberg, D.J. (1978) Specific volume measurements of Cu, Mo, Pd, and Ag and calibration of the ruby R_1 fluorescence pressure gauge from 0.06 to 1 Mbar. Journal of Applied Physics, 49, 3276.

Noguchi, N., Moriwaki, T., Ikemoto, Y., and Shinoda, K. (2012) OH group behavior and pressure-induced amorphization of antigorite examined under high pressure and temperature using synchrotron infrared spectroscopy. American Mineralogist, 97, 134–142.

Oberti, R., Hawthorne, F.C., Cannillo, E. and Cámara, F. (2007) Long-Range Order in Amphiboles. Reviews in Mineralogy and Geochemistry, 67, 124–171.

Parry, S. A., Pawley, A. R., Jones, R.L., and Clark, S.M. (2007) An infrared spectroscopic study of the OH stretching frequencies of talc and 10-A phase to 10 GPa. American Mineralogist, 92, 525–531.

Prewitt, C.T., and Parise, J.B. (2000) Hydrous Phases and Hydrogen Bonding at High Pressure. Reviews in Mineralogy and Geochemistry, 41, 309–333.

Rivers, M., Prakapenka, V., Kubo, A., Pullins, C., Holl, C., and Jacobsen, S. (2008) The COMPRES/GSECARS gas-loading system for diamond anvil cells at the Advanced Photon Source. High Pressure Research, 28, 273–292.

Robert, J.-L., Della Ventura, G., and Thauvin, J.-L. (1989) The infrared OH-stretching region of synthetic richterites. European Journal of Mineralogy, 1, 203–211.

Sano-Furukawa, A., Kagi, H., Nagai, T., Nakano, S., Fukura, S., Ushijima, D., Iizuka, R., Ohtani, E., and Yagi, T. (2009) Change in compressibility of delta-AlOOH and delta-AlOOD at high pressure: A study of isotope effect and hydrogen bond symmetrization, American Mineralogy, 94, 1255-1261.

Scott, H.P., Liu, Z., Hemley, R.J., and Williams, Q. (2007) High-pressure infrared spectra of talc and lawsonite. American Mineralogist, 92, 1814–1820.

Shieh, S.R., Duffy, T.S., Liu, Z., and Ohtani, E. (2009) High-pressure infrared spectroscopy of the dense hydrous magnesium silicates phase D and phase E. Physics of the Earth and Planetary Interiors, 175, 106–114.

Shim, S.-H., Rekhi, S., Martin, M., and Jeanloz, R. (2006) Vibrational spectroscopy and x-ray diffraction of Cd(OH)2 to 28GPa at 300K. Physical Review B, 74, 024107.

Stern, R.J. (2002) Subduction zones. Reviews of Geophysics, 40, 1012.

Strens, R.G.J. (1974) The common chain, ribbon and ring silicates. In V.C. Farmer, Ed., The Infrared Spectra of Minerals, p. 305–330. Mineralogical Society, London.

Tsuchiya, J., Tsuchiya T., and Tsuneyuki, S. (2005) First principles study of hydrogen bond symmetrization of phase D under high pressure, American Mineralogy, 90, 44–49.

Vinet, P., Ferrante, J., Rose, J.H. and Smith, J.R. (1987) Compressibility of solids. Journal of Geophysical Research, 92, 9319–9325.

Williams, Q., Knittle, E., Scott, H.P., and Liu, Z. (2012) The high-pressure behavior of micas: Vibrational spectra of muscovite, biotite, and phlogopite to 30 GPa. American Mineralogist, 97, 241–252.

Xu, W., Greenberg, E., Rozenberg, G.Kh., Pasternak, M.P., Bykova, E., Boffa-Ballaran, T., Dubrovinsky, L., Prakapenka, V., Hanfland, M., Vekilova, O.Yu., Simak, S.I., and Abrikosov, I.A. (2013) Pressure-induced hydrogen bond symmetrization in iron oxyhydride. Physical Review Letters, 111, 1-5.

Yang, H., Hazen, R.M., Prewitt, C.T., Finger, L.W., Lu, R., and Hemley, R.J. (1998) High-pressure single-crystal X-ray diffraction and infrared spectroscopic studies of the C2/*m*-$P2_1/m$ phase transition in cummingtonite. American Mineralogist, 83, 288–299.

Yang, X., Keppler, H., Dubrovinsky, L., and Kurnosov, A. (2014) In-situ infrared spectra of hydroxyl in wadsleyite and ringwoodite at high pressure and high temperature. American Mineralogist, 99, 724–729.

Figure Captions

Figure 1. Schematic of sample assemblies: **(a)** Previous studies which did not use a pressure medium or mix KBr with sample material were more likely to have preferred grain orientation, peak saturation, and larger pressure gradients; **(b)** Samples with KBr pressure medium and mixed KBr + sample platelets used in this study had reduced likelihood of grain orientation, peak saturation, and smaller pressure gradients; **(c)** Using mixed KBr + sample platelets while replacing KBr pressure medium with neon reduces deviatoric stresses, preserving sharper absorption peaks at high pressures.

Figure 2. Comparison of arfvedsonite (sample L30), anthophyllite (L31) and glaucophane (L24) peak occupations at ~12.5 GPa, with A, B, C, and D-bands corresponding to decreasing frequency. Circles indicate data points and dotted lines are the fitted peak shapes assigned based on that data.

Figure 3. High pressure, room temperature measurements of O-H frequencies within each sample composition in this study. Circles: individual peak positions. Different symbol colors are used for different compositions, and sample numbers appear in parenthesis. Compositional details available in Table 1. Error bars represent 1σ uncertainties both in frequency and in pressure.

Figure 4. Comparison of spectral peak widths using a non-hydrostatic KBr pressure medium versus a quasi-hydrostatic Ne pressure medium. Both sets of measurements were made using the same mineral specimen (tremolite). Sample L13 (blue markers) was loaded in Ne and sample L14 (red markers) was loaded using a KBr pressure medium. The same colors are used to identify samples within inset. Error bars represent 1σ uncertainties.

Figure 5. Comparison of pressure dependence of O-H stretching frequency in amphiboles and *t–o–t* (talc and mica-like) phyllosilicates. Closed circles: this study; different shades of infill indicate the A, B, C, and D bands as identified in Figure 2 and Table 1. Open circles: other amphiboles, talc, and micas. All of these minerals containing analogous hydrogen bonding sites, at the non-tetrahedral oxygen in *t–o–t* layers. Error bars represent 1σ uncertainties.

Figure 6. Comparison of pressure dependence of O-H stretching frequency in various minerals. Open circles: minerals containing only hydrogen bonding sites analogous to those in amphiboles. Cross symbols: minerals whose hydrogen accommodation mechanisms in the crystal structure are different from those in amphiboles. Open triangles: minerals containing both analogous and non-analogous hydrogen bonding sites. All literature data cited are from IR absorption studies, with the exception of Auzende et al. (2004), which used Raman spectroscopy.

Figure 7. Relationship between observed O-H frequency (cm^{-1}) and O-H bond length calculated from amphibole compressibility using a Vinet equation of state. The vertical axis is in units of frequency$^{(-2/3)}$ to illustrate that the data conform to Badger's rule, which predicts a linear relationship between $\omega^{-2/3}$ and r_e. Colors used here correspond to the same sample compositions as in Figure 3.

Tables

Table 1. Compositions of samples from energy-dispersive spectrometry (EDS); presented as cations per amphibole formula unit. All analyses are normalized to one hundred-oxide wt.% and are averages of 5-10 point analyses within individual grains. Numbers in parentheses are 1σ uncertainties on the last digit of each entry, and measured values smaller than 1σ deviations have been excluded from the table.

Sample	Na	Mg	Al	Si	Ca	Ti	Cr	Mn	Fe
L13, L14, tremolite	-	4.88(2)	0.06(2)	8.02(3)	1.76(2)	-	-	0.17(3)	-
L15, actinolite	-	4.35(2)	0.22(2)	7.91(3)	1.84(2)	-	0.05(2)	-	0.54(4)
L16, hornblende	-	4.34(2)	0.15(2)	7.96(3)	1.89(3)	-	0.03(2)	-	0.55(4)
L23, anthophyllite	0.15(2)	7.28(3)	3.41(3)	4.97(3)	-	-	-	-	0.56(4)
L24, glaucophane	1.75(2)	1.76(2)	1.10(2)	8.17(4)	0.06(1)	-	-	-	2.27(6)
R173, actinolite	0.21(2)	3.84(3)	0.33(2)	7.83(5)	2.02(4)	-	0.04(3)	-	0.78(6)
L26, L27, hornblende	0.72(2)	0.62(2)	6.04(4)	5.55(5)	0.03(2)	0.07(2)	-	-	1.66(8)
L30, arfvedsonite	2.77(2)	0.06(1)	0.23(1)	8.13(4)	0.04(1)	0.03(2)	-	0.16(3)	4.70(6)
L31, anthophyllite	0.10(2)	5.91(3)	-	8.44(3)	-	-	-	-	0.17(3)
L32, tremolite	0.32(2)	4.29(2)	0.19(2)	8.21(3)	1.77(3)	-	-	0.06(2)	-

Table 2. Pressure dependence of OH-frequencies within each sample. All values are in the units of $cm^{-1}GPa^{-1}$. Numbers in parentheses are 1σ uncertainties on the last digit of each entry.

Sample	D Band	C Band	B Band	A Band
L13, tremolite	-	-	-	1.43(04)
L14, tremolite	-	-	-	1.52(19)
L15, actinolite	-	-	1.03(17)	1.43(19)
L16, hornblende	-	-	0.92(13)	1.35(15)
L23, anthophyllite	-	-	-	2.32(19)
L24, glaucophane	0.26(08)	0.89(16)	1.33(16)	1.56(14)
R173, actinolite	-	0.07(06)	1.01(06)	1.63(03)
L26, hornblende	0.39(01)	0.37(05)	0.90(05)	1.34(04)
L27, hornblende	-0.30(04)	0.10(05)	1.08(14)	1.74(22)
L30, arfvedsonite	-0.33(01)	-0.04(04)	-	-
L31, anthophyllite	-	-	1.00(06)	1.43(08)
L32, tremolite	-	-	-	1.69(06)

Supplementary Table 1. Absorption peak positions, all values unless otherwise states in cm^{-1}. Spectral resolution for all measurements is 4 cm^{-1}. Pressure uncertainties on the last digit are in parentheses.

Sample	A band	B band	C band	D band	Pressure (GPa)
L13 (tremolite)	3682(4)	-	-	-	2.7(03)
	3686(4)	-	-	-	4.7(05)
	3689(4)	-	-	-	7.1(1)
	3692(4)	-	-	-	9.9(1)
	3697(4)	-	-	-	13.0(1)
	3701(4)	-	-	-	15.0(2)
	3703(4)	-	-	-	17.5(2)
	3707(4)	-	-	-	21.0(2)
	3710(4)	-	-	-	25.0(3)
	3714(4)	-	-	-	27.0(3)
	3719(4)	-	-	-	31.5(3)
	3720(4)	-	-	-	34.0(3)
	3723(4)	-	-	-	37.0(4)
	3727(4)	-	-	-	41.0(4)
	3730(4)	-	-	-	43.1(4)
	3733(4)	-	-	-	45.1(5)
	3734(4)	-	-	-	48.0(5)
	3736(4)	-	-	-	51.2(5)
	3737(4)	-	-	-	54.0(5)
	3743(4)	-	-	-	56.0(6)
	3733(4)	-	-	-	58.1(6)
L14 (tremolite)	3674(4)	-	-	-	0.4(02)
	3677(4)	-	-	-	1.5(08)
	3683(4)	-	-	-	3.4(2)
	3693(4)	-	-	-	8.5(4)
	3698(4)	-	-	-	13.5(7)
	3701(4)	-	-	-	18.6(9)
	3709(4)	-	-	-	24.0(12)
	3715(4)	-	-	-	30.1(15)
	3719(4)	-	-	-	37.0(19)
L15 (actinolite)	3679(4)	3663(4)	-	-	3.1(2)
	3686(4)	3669(4)	-	-	6.0(3)
	3694(4)	3671(4)	-	-	11.2(6)
	3698(4)	3677(4)	-	-	14.0(7)
	3699(4)	3678(4)	-	-	17.5(9)
	3702(4)	3678(4)	-	-	21.5(11)
	3711(4)	3684(4)	-	-	28.5(14)

	3709(4)	3685(4)	-	-	32.5(16)
	3722(4)	3693(4)	-	-	39.5(20)
	3726(4)	3694(4)	-	-	43.0(22)
	3731(4)	3693(4)	-	-	48.0(24)
	3733(4)	3690(4)	-	-	52.5(26)
	3737(4)	3696(4)	-	-	56.5(28)
	3738(4)	3695(4)	-	-	60.5(30)
L16 (hornblende)	3695(4)	3663(4)	-	-	3.0(2)
	3686(4)	3670(4)	-	-	7.8(4)
	3694(4)	3671(4)	-	-	11.5(6)
	3702(4)	3679(4)	-	-	19.5(10)
	3718(4)	3687(4)	-	-	28.5(14)
	3729(4)	3697(4)	-	-	34.0(17)
	3726(4)	-	-	-	40.1(20)
L23 (anthophyllite)	3676(4)	-	-	-	0.7(01)
	3678(4)	-	-	-	1.8(02)
	3680(4)	-	-	-	3.2(03)
	3683(4)	-	-	-	4.8(05)
	3698(4)	-	-	-	10.0(1)
L24 (glaucophane)	-	3664(4)	3649(4)	3618(4)	1.1(01)
	-	3676(4)	3660(4)	3621(4)	7.0(07)
	-	3884(4)	3667(4)	3622(4)	12.7(1)
	-	-	3672(4)	3622(4)	17.8(2)
	-	-	3677(4)	3622(4)	20.6(2)
	-	-	3687(4)	-	30.7(3)
	-	-	3690(4)	-	38.0(4)
	-	-	3689(4)	-	42.2(4)
R173 (actinolite)	3678(4)	3663(4)	3648(4)	-	2.0(1)
	3680(4)	3666(4)	3649(4)	-	3.3(2)
	3682(4)	-	-	-	4.5(2)
	3691(4)	3672(4)	-	-	10.0(5)
	3694(4)	3674(4)	3648(4)	-	12.5(6)
	3697(4)	3675(4)	-	-	13.8(7)
	3701(4)	3679(4)	3649(4)	-	16.3(8)
	3711(4)	3676(4)	3649(4)	-	23.5(12)
	3719(4)	3687(4)	3656(4)	-	31.5(16)
	3720(4)	3689(4)	-	-	33.8(17)
	3724(4)	3693(4)	-	-	36.5(18)
	3726(4)	3693(4)	-	-	38.3(19)
	3727(4)	-	-	-	40.5(20)
	3728(4)	-	-	-	43.3(22)
	3730(4)	-	-	-	44.8(22)
	3732(4)	-	-	-	47.5(24)
L26 (hornblende)	3673(4)	3659(4)	3647(4)	3622(4)	1.2(06)
	3676(4)	3661(4)	3648(4)	3623(4)	3.0(2)
	3681(4)	3665(4)	3650(4)	-	6.5(3)
	3684(4)	3666(4)	3651(4)	-	8.5(4)
	3692(4)	3672(4)	3653(4)	-	15.3(8)
	3696(4)	3674(4)	3653(4)	-	18.1(9)
	3702(4)	3675(4)	-	-	23.0(12)
	3710(4)	-	-	-	28.5(14)
L27 (hornblende)	3675(4)	3659(4)	3649(4)	3620(4)	2.3(1)
	3679(4)	3662(4)	3648(4)	3620(4)	3.0(2)
	3681(4)	3667(4)	3649(4)	3620(4)	6.3(3)
	3691(4)	3673(4)	3649(4)	3620(4)	13.1(7)
	-	-	3651(4)	3620(4)	16.8(8)
	3703(4)	3676(4)	3650(4)	3620(4)	22.9(11)
	3710(4)	-	3650(4)	3620(4)	27.8(14)
L30 (arfvedsonite)	-	-	3649(4)	3620(4)	9.2(5)
	-	-	3649(4)	3619(4)	12.9(6)
	-	-	-	3617(4)	16.1(8)
	-	-	3649(4)	3616(4)	20.0(10)
	-	-	3649(4)	3611(4)	24.5(12)
	-	-	3649(4)	3606(4)	28.4(14)
	-	-	3649(4)	3601(4)	32.6(16)
	-	-	3649(4)	3597(4)	36.2(18)
	-	-	3649(4)	3597(4)	38.3(19)
	-	-	3649(4)	3596(4)	40.6(20)
	-	-	3649(4)	3595(4)	43.0(22)
L31 (anthophyllite)	3683(4)	3665(4)	-	-	5.3(3)

	3684(4)	3665(4)	-	-	6.8(3)
	3687(4)	3667(4)	-	-	9.2(5)
	3690(4)	3670(4)	-	-	10.8(5)
	3693(4)	3672(4)	-	-	12.3(6)
	3696(4)	3674(4)	-	-	14.7(7)
	3703(4)	3678(4)	-	-	19.9(10)
	3714(4)	-	-	-	22.1(11)
	3732(4)	-	-	-	30.2(15)
	3741(4)	-	-	-	33.0(17)
	3761(4)	-	-	-	37.3(19)
	3776(4)	-	-	-	39.8(20)
	3788(4)	-	-	-	43.0(22)
	3799(4)	-	-	-	46.2(23)
	3809(4)	-	-	-	48.5(24)
	3823(4)	-	-	-	50.6(25)
L32 (tremolite)	3682(4)	-	-	-	4.4(2)
	3683(4)	-	-	-	6.4(3)
	3689(4)	-	-	-	8.9(4)
	3691(4)	-	-	-	10.2(5)
	3693(4)	-	-	-	11.5(6)
	3693(4)	-	-	-	12.7(6)
	3698(4)	-	-	-	14.1(7)
	3701(4)	-	-	-	15.7(8)
	3705(4)	-	-	-	18.4(9)
	3710(4)	-	-	-	22.9(11)
	3716(4)	-	-	-	28.9(14)
	3719(4)	-	-	-	32.3(16)
	3722(4)	-	-	-	35.5(18)
	3724(4)	-	-	-	37.8(19)
	3729(4)	-	-	-	42.8(21)
	3732(4)	-	-	-	45.4(23)

Fig. 1

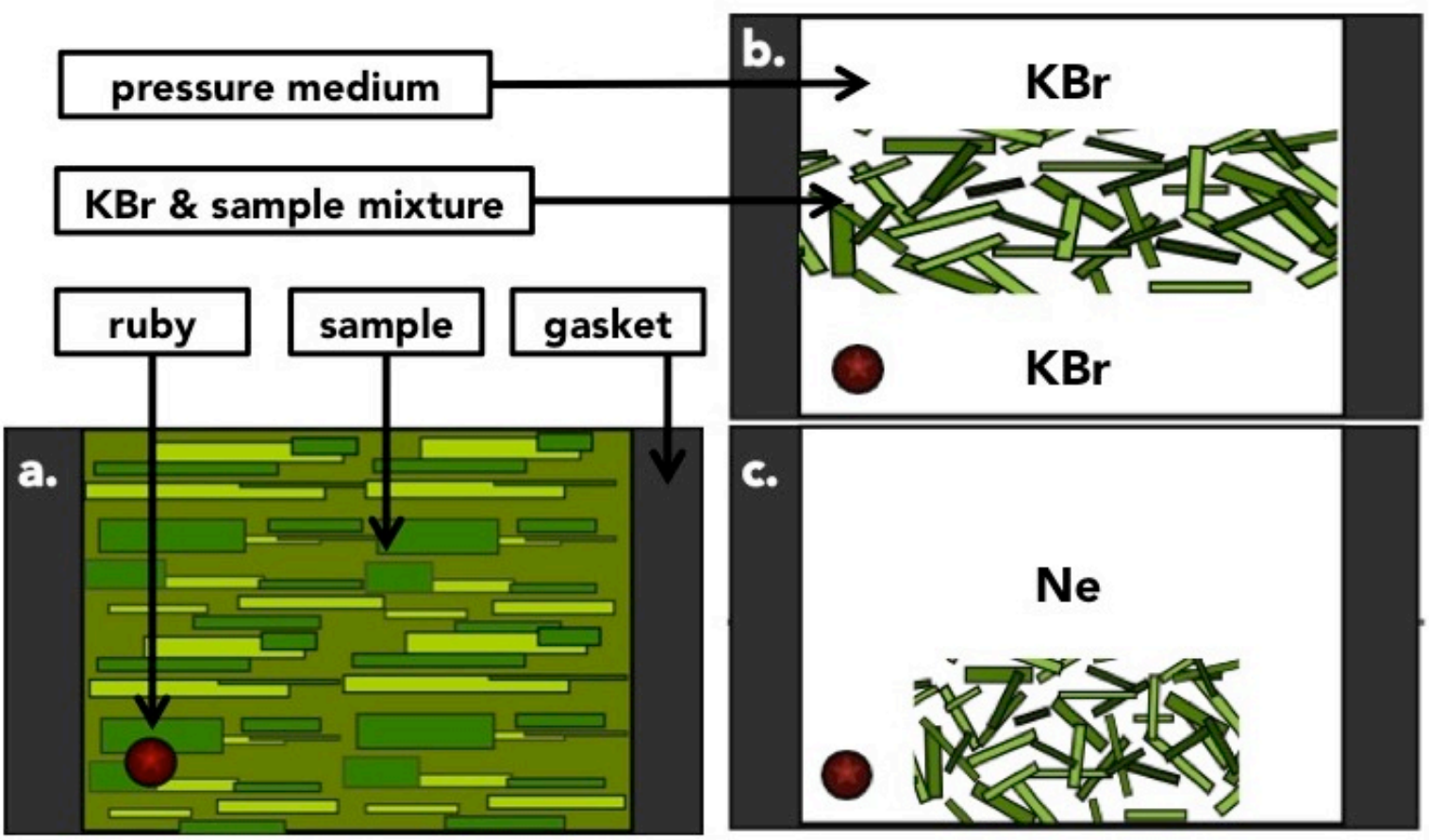
pressure medium
KBr & sample mixture
ruby
sample
gasket
a.
b.
KBr
KBr
c.
Ne

Fig. 2

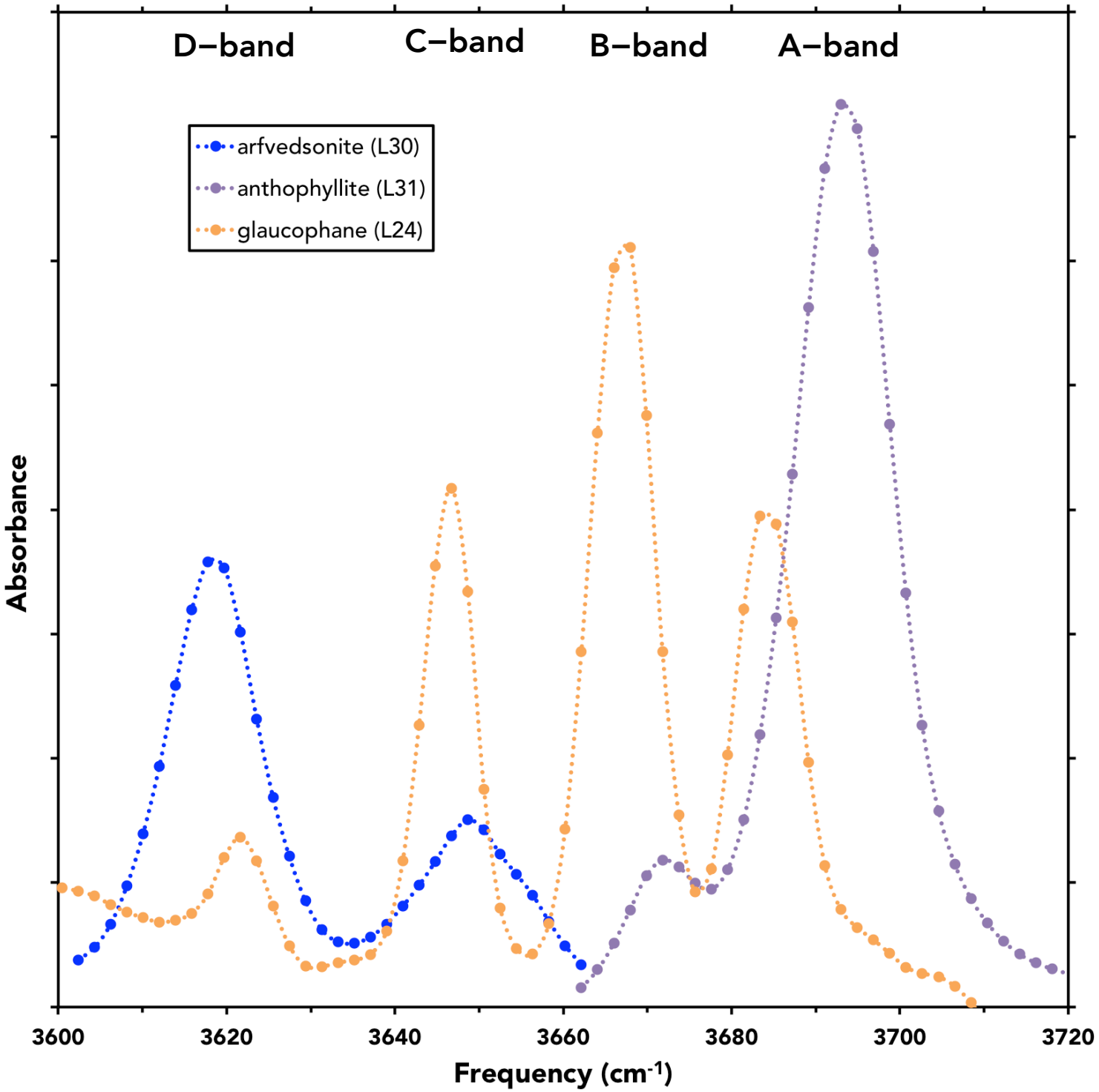
D–band
C–band
B–band
A–band
arfvedsonite (L30)
anthophyllite (L31)
glaucophane (L24)
Absorbance
3600
3620
3640
3660
3680
3700
3720
Frequency (cm-1)

Fig. 3

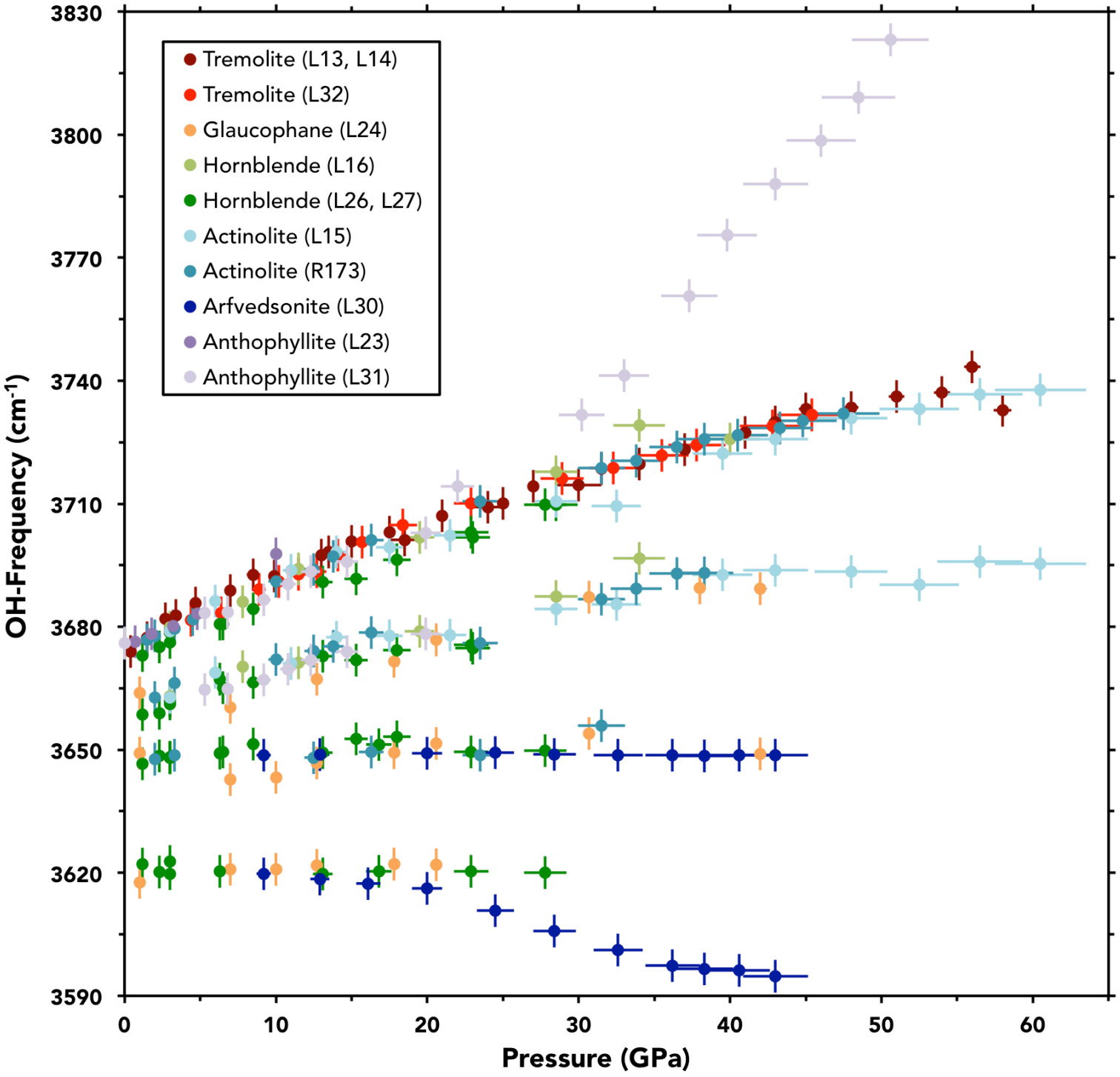
Tremolite (L13, L14)
Tremolite (L32)
Glaucophane (L24)
Hornblende (L16)
Hornblende (L26, L27)
Actinolite (L15)
Actinolite (R173)
Arfvedsonite (L30)
Anthophyllite (L23)
Anthophyllite (L31)
OH-Frequency (cm-1)
3830
3800
3770
3740
3710
3680
3650
3620
3590
0
10
20
30
40
50
60
Pressure (GPa)

Fig. 4

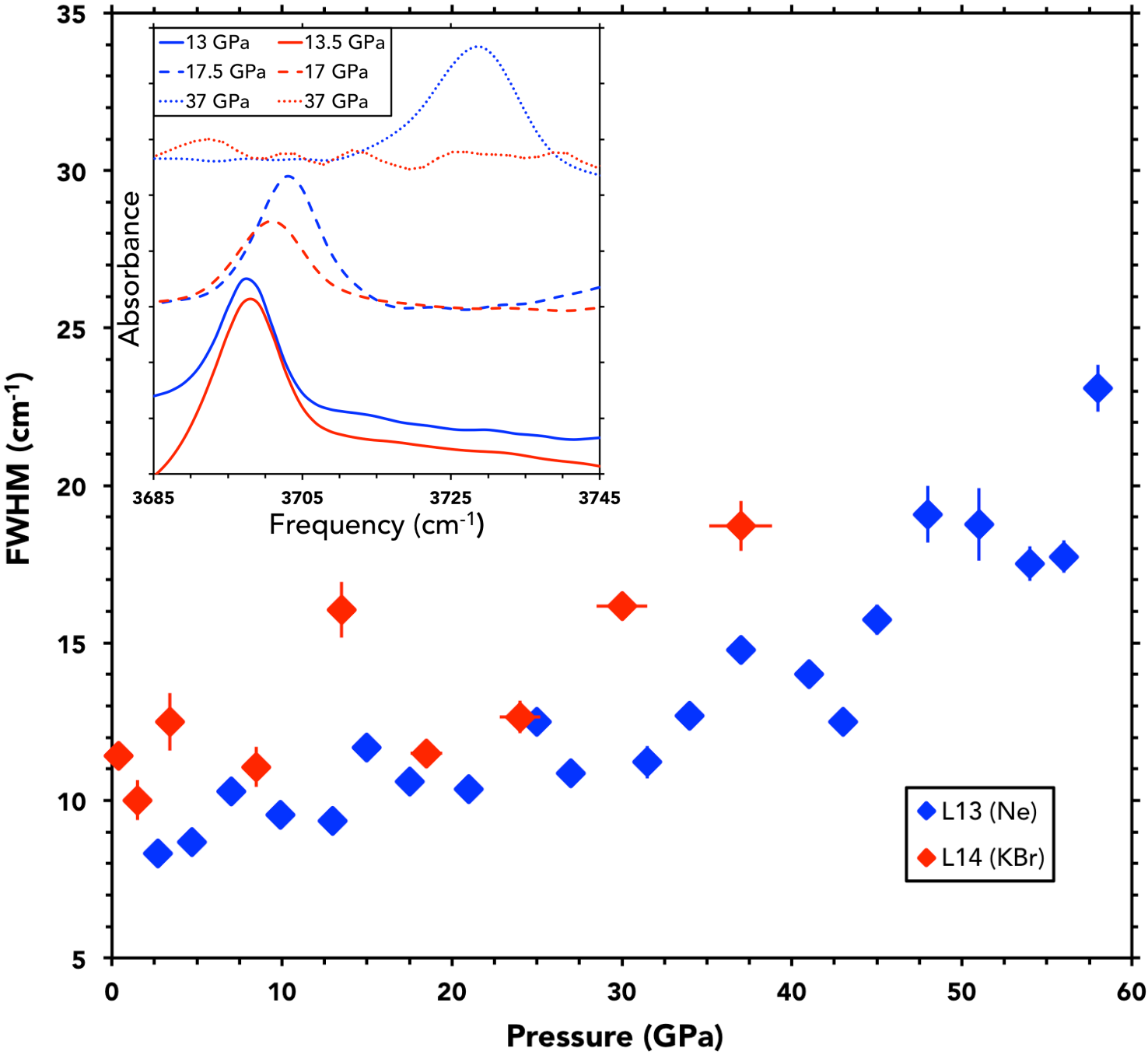
FWHM (cm-1)
Pressure (GPa)
L13 (Ne)
L14 (KBr)
Absorbance
Frequency (cm-1)
13 GPa
13.5 GPa
17.5 GPa
17 GPa
37 GPa
37 GPa

Fig. 5

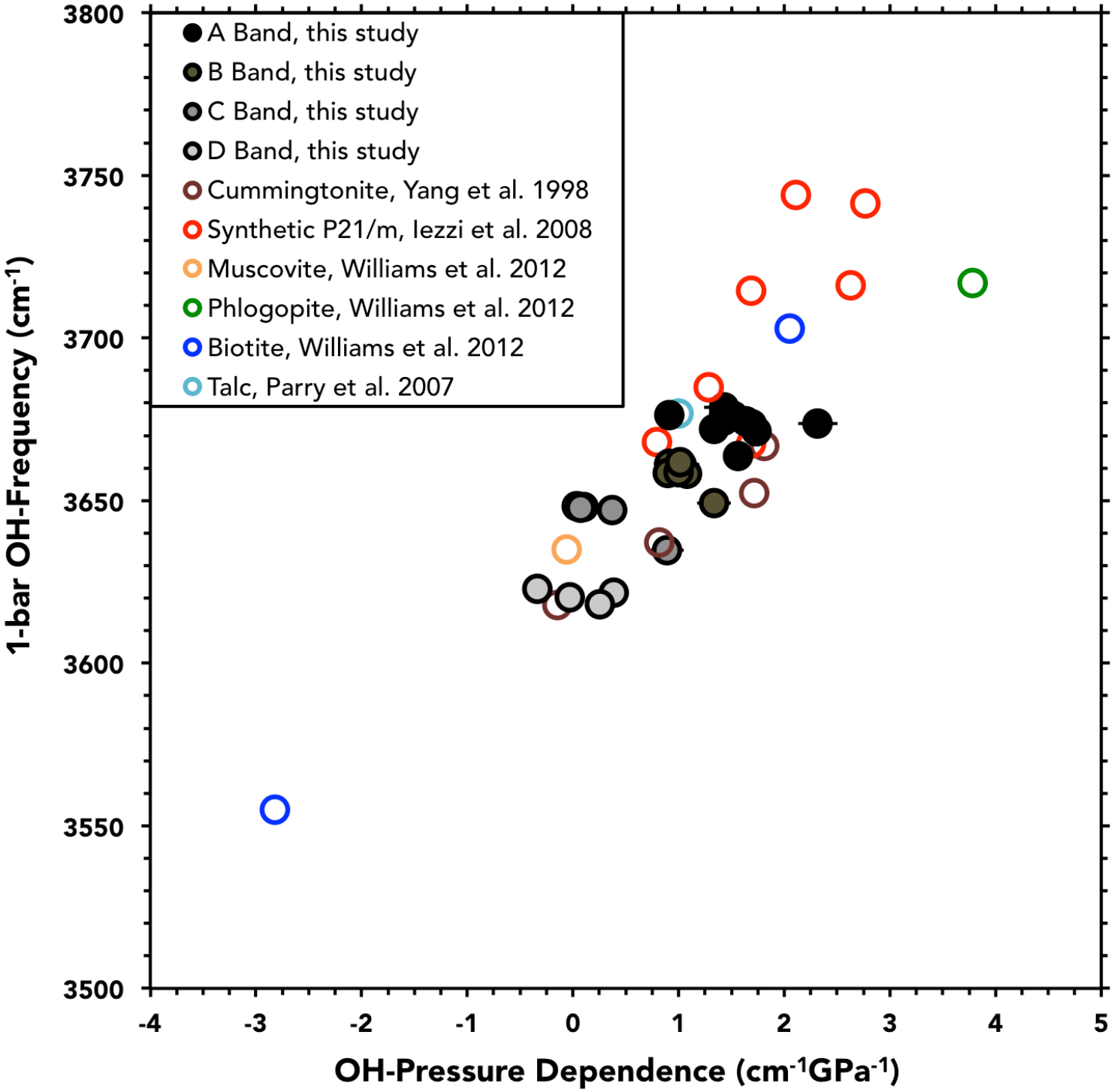
A Band, this study
B Band, this study
C Band, this study
D Band, this study
Cummingtonite, Yang et al. 1998
Synthetic P21/m, Iezzi et al. 2008
Muscovite, Williams et al. 2012
Phlogopite, Williams et al. 2012
Biotite, Williams et al. 2012
Talc, Parry et al. 2007
3800
3750
3700
3650
3600
3550
3500
-4
-3
-2
-1
0
1
2
3
4
5
1-bar OH-Frequency (cm-1)
OH-Pressure Dependence (cm-1GPa-1)

Fig. 6

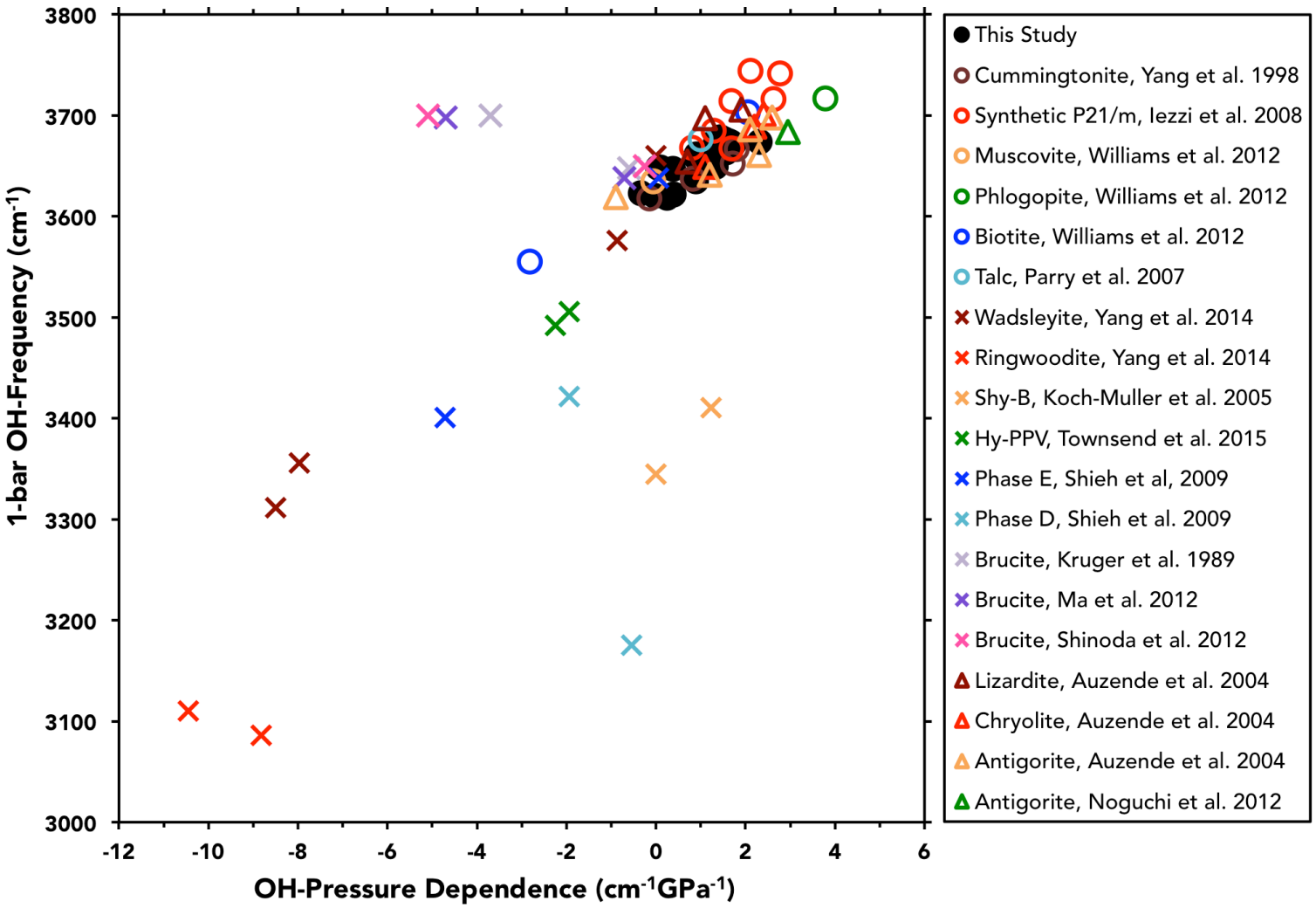
3800
3700
3600
3500
3400
3300
3200
3100
3000
1-bar OH-Frequency (cm-1)
-12
-10
-8
-6
-4
-2
0
2
4
6
OH-Pressure Dependence (cm-1GPa-1)
This Study
Cummingtonite, Yang et al. 1998
Synthetic P21/m, Iezzi et al. 2008
Muscovite, Williams et al. 2012
Phlogopite, Williams et al. 2012
Biotite, Williams et al. 2012
Talc, Parry et al. 2007
Wadsleyite, Yang et al. 2014
Ringwoodite, Yang et al. 2014
Shy-B, Koch-Muller et al. 2005
Hy-PPV, Townsend et al. 2015
Phase E, Shieh et al, 2009
Phase D, Shieh et al. 2009
Brucite, Kruger et al. 1989
Brucite, Ma et al. 2012
Brucite, Shinoda et al. 2012
Lizardite, Auzende et al. 2004
Chryolite, Auzende et al. 2004
Antigorite, Auzende et al. 2004
Antigorite, Noguchi et al. 2012

Fig. 7

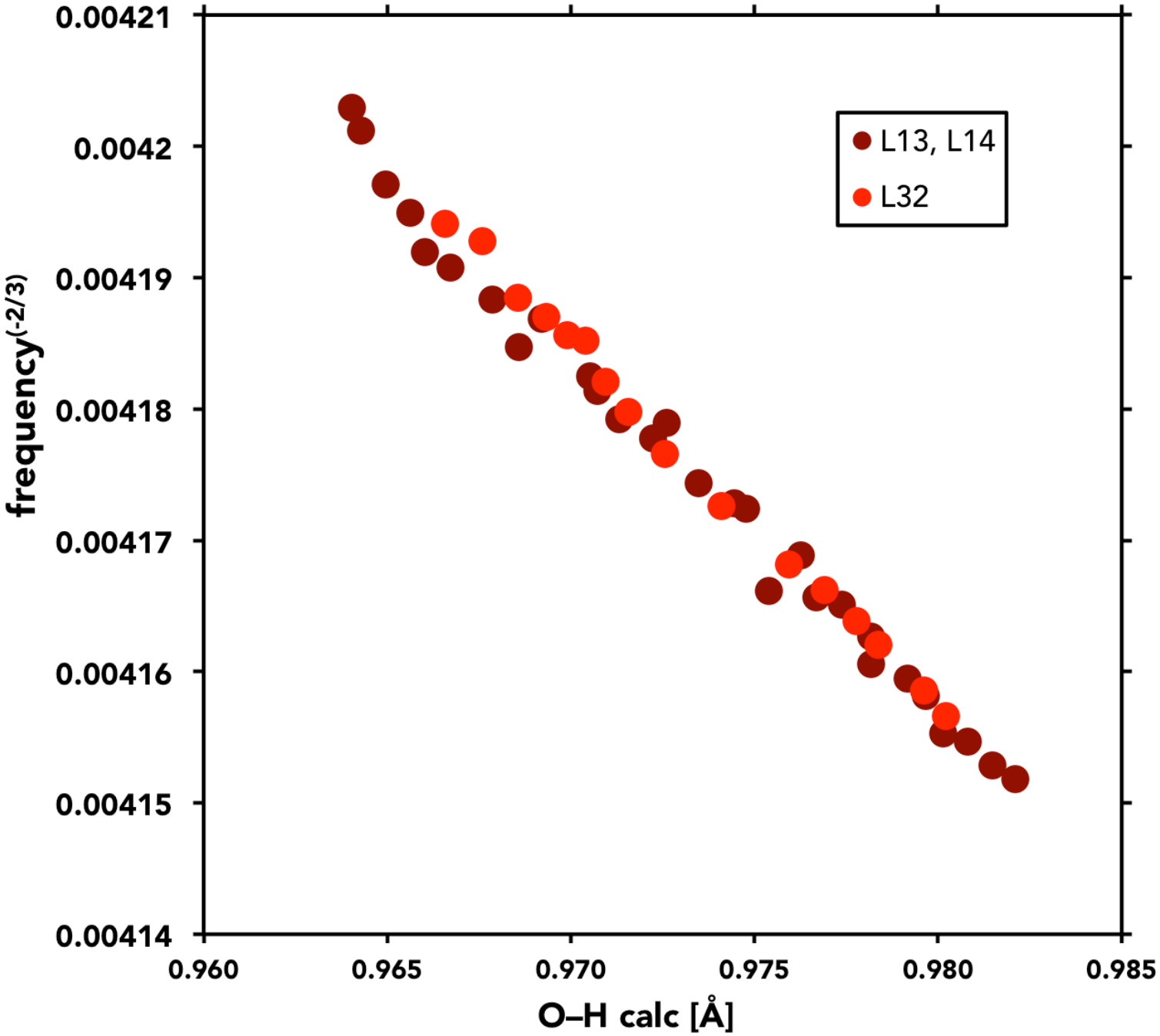
0.00421
0.0042
0.00419
0.00418
0.00417
0.00416
0.00415
0.00414
frequency(-2/3)
0.960
0.965
0.970
0.975
0.980
0.985
O–H calc [Å]
L13, L14
L32